Physica B 513 (2017) 48–57

Contents lists available at ScienceDirect

Physica B

journal homepage: www.elsevier.com/locate/physb

Femtosecond laser fluence based nanostructuring of W and Mo in ethanol

Shazia Bashir[a,b,*], Muhammad Shahid Rafique[a,c], Chandra Sekher Nathala[a], Ali Asghar Ajami[a,d], Wolfgang Husinsky[a]

[a] Institute of Applied Physics, Vienna University of Technology, Vienna, Austria
[b] Centre for Advanced Studies in Physics, Government College University Lahore, Pakistan
[c] Department of Physics, University of Engineering and Technology Lahore, Pakistan
[d] Faculty of Physics, Semnan University, Semnan, Iran

ARTICLE INFO

Keywords:
Femtosecond laser
Tungsten
Molybdenum
Laser fluence
Surface modification
Laser induced periodic surface structures

ABSTRACT

The effect of femtosecond laser fluence on nanostructuring of Tungsten (W) and Molybdenum (Mo) has been investigated after ablation in ethanol environment. A Ti: Sapphire laser (800 nm, 30 fs) at fluences ranging from 0.6 to 5.7 J cm^{-2} was employed to ablate targets. The growth of structures on the surface of irradiated targets is investigated by Field Emission Scanning Electron Microscope (FESEM) analysis. The SEM was performed for both central as well as the peripheral ablated regions. It is observed that both the development and shape of nanoscale features is dependent upon deposited energies to the target surface as well as nature of material. Nanostructures grown on Mo are more distinct and well defined as compared to W. At central ablated areas of W, unorganized Laser Induced Periodic Surface Structures (LIPSS) are grown at low fluences, whereas, nonuniform melting along with cracking is observed at higher fluences. In case of Mo, well-defined and organized LIPSS are observed for low fluences. With increasing fluence, LIPSS become unorganized and broken with an appearance of cracks and are completely vanished with the formation of nanoscale cavities and conical structures. In case of peripheral ablated areas broken and bifurcated LIPSS are grown for all fluences for both materials. The, ablated diameter, ablation depth, ablation rate and the dependence of periodicity of LIPSS on the laser fluence are also estimated for both W and Mo. Parametric instabilities of laser-induced plasma along with generation and scattering of surface plasmons is considered as a possible cause for the formation of LIPSS. For ethanol assisted ablation, the role of bubble cavitation, precipitation, confinement and the convective flow is considered to be responsible for inducing increased hydrodynamic instabilities at the liquid-solid interface.

1. Introduction

Laser induced micro/nano-structuring of materials is a versatile tool to modify the properties of materials for enhanced optical absorption [1], thermal [2], field emission [3], hydrophobicity [4], biocompatibility [5] and tribological performance [6]. A large variety of complex and multiscale features e.g. Laser Induced Periodic Surface Structures (LIPSSs) [7], pillars [8], naonocracks [9], nanodots [10], nanopores or nanocavities [11] and leaf-like nanoplatelets [12] can be grown on surfaces of solids by using femtosecond lasers. LIPSS or ripples have been extensively studied since the first discovery by Birnbaum on semiconductor surfaces [13]. A large number of previous reports confirmed that this could be recognized as a general phenomenon of laser-matter interaction on diverse kind of materials e.g. metals, semiconductors and dielectrics [13–16]. Several theories such as radiation remnants, second harmonic generation, or plasmonic excitations, Coulomb explosion and parametric decay model have been proposed for growth mechanism of LIPSS during ultrafast laser ablation [15–17]. However, the mechanism is not yet completely understood and remains a topic of debate.

Laser ablation-based nanofabrication is strongly dependent upon laser beam parameters, such as wavelength, pulse duration, fluence and nature of material as well the environmental conditions and their nanochemical effects [18,19]. The ablation efficiency of materials is significantly influenced by offering different cooling and quenching rates, confinement and shielding effects, shock wave generation and chemical reactivity of the environment [19,20]. Various physical processes such as plasma formation, condensation, agglomeration, nucleation and coalescence are responsible for generation, growth and size of nanostructures in the presence of reactive environment [21].

Femtosecond laser assisted ablation and deposition of W and Mo

* Corresponding author at: Centre for Advanced Studies in Physics, Government College University Lahore, Near Secretariat, Church Road, Pakistan.
E-mail address: shaziabashir@gcu.edu.pk (S. Bashir).

http://dx.doi.org/10.1016/j.physb.2017.03.008
Received 29 November 2016; Received in revised form 1 March 2017; Accepted 2 March 2017
Available online 03 March 2017

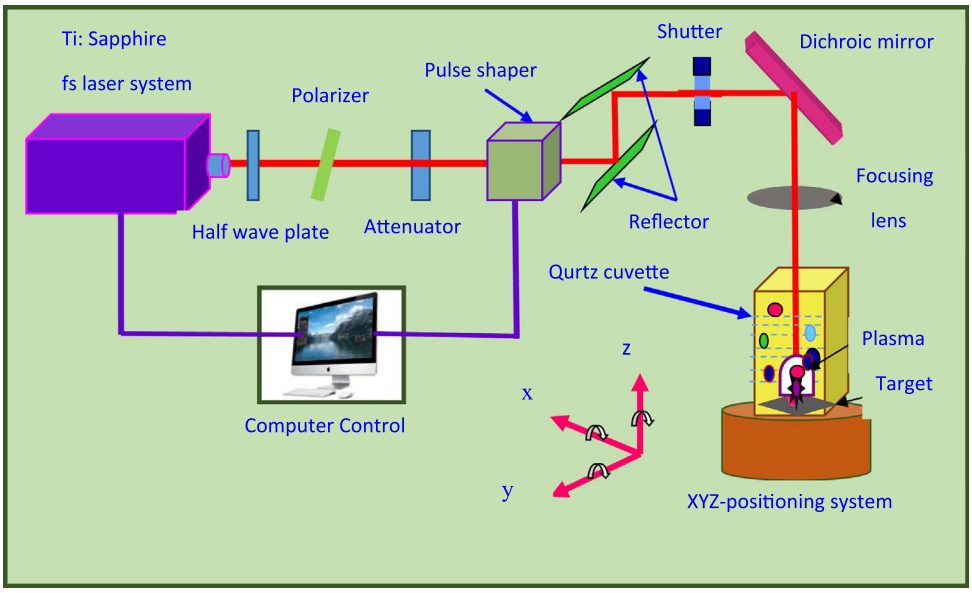

Fig. 1. The schematic of experimental set-up for exposure of W and Mo by fs laser pulses in ethanol environment.

has been reported by many researchers [11–13]. The hydrothermal treatment during laser assisted ablation provides an effective synthetic approach for fabrication of morphologically tunable WO_3 nanomaterials, with promising applications in gas sensing, electrochromic devices and photocatalysis [22]. W is widely used as filaments, electrodes, electrical and electronic contacts. Mo metal and its alloys have specialized applications due to unique combination of properties, including high strength at elevated temperatures, high thermal and electrical conductivity, and low thermal expansion. Zhang *et al.* reported that MoS_2 exhibits significant saturable absorption under femtosecond laser excitation at 800 nm and is potential candidate for ultrafast photonics [22]. Femtosecond laser interaction with metallic W is reported by Fujimoto et al. [23]. The deposition of W nanogratings induced by a single femtosecond laser beam has been reported by Zhang et al. [24]. Laser-assisted nanostructuring of W in liquid environment [20] and improvement in thermionic properties is investigated by Barmina et al. [2]. Femtosecond laser-induced periodic surface structure formation on W is reported by Vorobyev and Guo [25]. Tang et al. [26] reported that the self-assembled, highly uniform and tuneabale W nanogratings initiated by a single femtosecond pulsed laser can be controlled by controlling the laser power and scanning speed. Sub wavelength dot-like structures are directly generated on Mo surfaces by focusing two-color femtosecond laser pulses [27]. Nanoscale cracks oriented perpendicular to the incident laser polarization are induced by low fluence femtosecond laser irradiation on metallic surfaces of W, Mo and Cu. Their formation is attributed to local filed enhancement around the nanoscale holes on the metal surface [9].

The purpose of the present work is to investigate the effect of variation in femtosecond laser fluence on nanostructuring of W and Mo in the ethanol environment. The threshold fluence, ablated diameter, ablation depth, ablation rate, and the dependence of the periodic structure interspaces on the laser fluence are measured experimentally and are compared with theoretically calculated or reported values by other groups. The motivation behind this wok was to explore: effect of the peak fluence as well local fluence on the formation of nanostructures, material response (enthalpy of evaporation, thermal conductivity, reflectivity, absorption coefficient, melting point for W and Mo,), as well as effect of wet (ethanol) ablation on the surface modifications after fs laser irradiation. Laser ablation of W and Mo in ethanol introduces various nonlinear effects and enhances thermal and chemical reactivity at the solid-liquid interface due to confinement. A Ti: Sapphire laser with central wavelength of 800 nm, pulse duration of 30 fs at various peak fluences ranging from 0.6 to 5.7 J cm^{-2} was employed as an irradiation source for ablation of W and Mo in ethanol. Field Emission Scanning Electron Microscope (FESEM) analysis was performed to explore the nano structures formed on the surface of the ablated W and Mo. To evaluate ablation rate, the crater depth was measured with a confocal microscope.

2. Experimental

The present work deals with the ablation of W and Mo with multiple femtosecond laser pulses irradiation in ethanol. The grinded, polished and ultrasonically cleaned W and Mo specimens with dimensions of 10 mm×10 mm×10 mm×3 mm were mounted on the motorized xyz- manipulator to position the targets precisely for each exposure.

A regenerative Chirp Pulse Amplified (CPA) with central wavelength of λ_L 800 nm, Ti: Sapphire laser system (Femtolasers, Compact Pro) with a pulse duration of 30 fs at 1 kHz repetition rate (1.5 eV single photon energy) was used for irradiation. The pulse energy was measured using a power energy meter (a pyroelectric detector Coherent) in front of the liquid cell (filled with ethanol) that was placed before the lens and the energy was varied using neutral density filters and a linear polarizer.

Both the targets of W and Mo were exposed in ethanol, for nine laser pulsed energies of 50, 100, 150, 200, 250, 300, 350, 400 and 450 μJ, while keeping the pulse duration constant at 30 fs. These energies correspond to peak laser fluences of 0.6, 1.3, 1.9, 2.5, 3.2, 3.8, 4.4, 5 and 5.7 J cm^{-2} respectively. Targets were immersed in ethanol filled in a quartz cuvette in such a way that the target was lying on the bottom of the cuvette. The laser beam was brought through the top of the quartz cuvette to avoid the energy losses by the cuvette.

Each exposure was done with 1000 number of pulses. The laser pulses were directed at normal incidence onto the target surface. The schematic of experimental set-up is shown in Fig. 1. The laser intensity distribution was adjusted to be spatially uniform by using a Gaussian profile. The laser beam was subsequently focused using a lens of focal length 20 cm. The target was placed at 2.7 mm before the focal position to avoid filamentation of laser pulses in ethanol at the focus point. The laser spot size on the target was 100 μm in diameter.

The surface morphology of the irradiated W and Mo was analyzed by using a Field Emission Scanning Electron Microscope (SEM, FEI-

QUANTA 200 F, Netherlands). SEM analysis was performed for both central as well as for peripheral ablated regions of W and Mo.

For exploring the surface morphology of peripheral ablated areas, the SEM analysis was performed at 100 μm away from central position where local fluence are evaluated.

The ablation threshold fluence is determined by fitting the laser fluence dependence of ablation rate. To evaluate ablation rate, we measured crater depth with a confocal laser scanning microscope (Nano focus μsurf explorer version 7.02).

3. Results and discussion

Femtosecond laser ablation of W and Mo at wavelength of 800 nm, number of pulses 1000, pulse duration of 30 fs in ethanol at various fluences was carried out. The value of peak fluence ranges from 0.6 J cm^{-2} to 5.7 J cm^{-2} and local fluence ranges from 0.2 m J cm^{-2} to 1.9 m J cm^{-2}. The local fluences at the peripheries at a distance of 100 μm (radius of sphere) from centre, exactly where growth of LIPSS is observed have been evaluated by using following relation [28].

$$\varnothing_{min} \approx \varnothing_o \exp\left[-1/2\left(\frac{D_{LIPSSo}}{\omega_0}\right)^2\right] \quad (1)$$

where $\varnothing_{min}$*is*is the local fluence, $\varnothing_o$ is the peak fluence, D_{LIPSSo} is diameter of peripheral region (200 μm for present case), where surface structures are observed, $\omega_0$is beam waist. The evaluated values of local fluences therefore decrease to ~0.3×10^{-3} from the peak fluence. A significant drop of the fluence range is seen specifically for from the centre into the periphery of the craters.

The evaluated values of local fluences are 0.2, 0.4, 0.6, 0.8, 1, 1.3, 1.5, 1.7, and 1.9 m J cm^{-2}.

3.1. Surface analyses of W

The fluence calculated at the central location of the laser spot (central ablated region) has been termed as peak fluence whereas the fluence at the periphery of the spot is named as local fluence. SEM images in Fig. 2(a–i) reveal the variation in the surface morphology of central ablated regions of W targets, exposed to 1000 laser pulses in ethanol, for various peak laser fluences of (a) 0.6 J cm^{-2}, (b) 1.3 J cm^{-2}, (c) 1.9 J cm^{-2}, (d) 2.5 J cm^{-2}, (e) 3.2 J cm^{-2}, (f) 3.8 J cm^{-2}, (g) 4.4 J cm^{-2}, (h) 5 J cm^{-2}and (i) 5.7 J cm^{-2}.

Nonuniform and unorganized LIPSS are observed in the central ablated areas at low fluences ranging from 0.6 to 2.5 J cm^{-2}(Fig. 2a–d). These LIPSS are covered with small scale pores which are arranged in perpendicular direction to LIPSS. When the fluence is increased to 3.2 J cm^{-2}, (Fig. 2e) LIPSS are partially vanished with significant cracking. With further increase in laser fluence from 3.8 to 5.7 J cm^{-2}, LIPSS are completely vanished and nonuniform melting along with nano cracking is observed in Fig. 2(f–i). The origin of such kind of unidirectional nanocracks formed on metallic surfaces of W and Mo at low-fluence of femtosecond laser pulses is the locally enhanced electric field along the direction perpendicular to the incident laser polarization around a nanoscale hole [29].

SEM images in Fig. 3(a–i) correspond to the variation in the surface morphology of peripheral ablated areas of W targets, exposed to 1000 laser pulses in ethanol, for various local laser fluences of (a) 0.2 m J cm^{-2}, (b) 0.4 m J cm^{-2}, (c) 0.6 m J cm^{-2}, (d) 0.8 m J cm^{-2}, (e) 1.00 m J cm^{-2}, (f) 1.3 m J cm^{-2}, (g) 1.5 m J cm^{-2}, (h) 1.7 m J cm^{-2}and (i) 1.9 m J cm^{-2}. LIPSS at all laser fluences are formed at the peripheral ablated of areas of W. In the peripheral ablated areas, significantly unorganized, undefined, bifurcated and broken ripples are viewed. The uniformity increases with increasing laser fluences and LIPSS with maximum distinctness and uniformity are seen at a fluence of 1.7 m J cm^{-2} (Fig. 3h).

LIPSS formation is attributed to the stimulated growth of a particular spatial component of small surface roughness that is selected by the phase-matching condition during light scattering at the metal surface. The scattering of the incident light via the surface roughness generates surface plasmon wave, which interferes with the incident light and produces standing wave pattern on the surface. Such surface standing wave induces periodic deposition of metal and serves as grating components to scatter more incident light into surface plasmon wave. A positive feedback loop is thus established between the initial surface roughness and surface plasmon wave, resulting in the spontaneous formation of surface periodic structures [11].

For liquid assisted ablation, bubble expansion/collapse precipitates the convective flow of the metallic molten layer due to variations in surface tension (thermocapillary effect) of the material [2,18]. These variations are responsible for inducing increased hydrodynamic instabilities called Kelvin-Helmholtz and pressures at the liquid-solid interface [5]. In liquids extreme pressure and temperature conditions in the focal volume during laser ablation, enhances the thermal stresses and generation of shock waves in W and Mo. The relaxation of these thermal stresses is rapid in ethanol than in air due to high density medium and hence supports the formation of cracking along with small scale structures such as droplets, pores and colloids [10].

The possible mechanism for the formation of nanoscale particulates, droplets and branches is hydrodynamical instability which is caused by the variations in surface tension gradients at liquid-solid interface [15].

3.2. Surface analyses of Mo

SEM micrographs in Fig. 4(a–i) show the variation in the surface morphology of central ablated regions of Mo targets, exposed to 1000 laser pulses in ethanol, for various peak laser fluences of (a) 0.6 J cm^{-2}, (b) 1.3 J cm^{-2}, (c) 1.9 J cm^{-2}, (d) 2.5 J cm^{-2}, (e) 3.2 J cm^{-2}, (f) 3.8 J cm^{-2}, (g) 4.4 J cm^{-2}, (h) 5 J cm^{-2}and (i) 5.7 J cm^{-2}.

Distinct LIPSSs on the surface of Mo exposed at low fluences ranging from 0.6 J cm^{-2} to 1.9 J cm^{-2} are exhibited in Figs. 4(a)–(c). The distinctness of LIPSS increases with increasing fluence. The moderate fluence regime ranging from 2.5 J cm^{-2} to 3.8 J cm^{-2} (Figs. 4d–f) is responsible for partial destruction of LIPSS along with the growth of cracks. The high laser fluence ranging from 4.4 J cm^{-2} to 5.7 J m^{-2} is responsible for complete termination of LIPSS. and formation of nanocavities as shown in Figs. 4(g)–(i). The diameter as well as the distinctness of cavities significantly increase with increasing fluence.

Surface structures grown with peak laser fluences ranging from 0.6 J cm^{-2} to 5.7 J cm^{-2} are seen to differ greatly depending upon the extent of the fluence. The surface features formed at lower laser fluence regime are LIPSS. Structures formed at a moderate laser fluence are nanocracks. Whereas, features at high fluence regime are nano cavities and pits. With increasing laser fluence (within high regime), both the size and density of nanoscale cavities, pits or cones increase. This is attributed to increased absorption by nanoparticles on the surface produced by preceding pulses as well as geometric effects caused by scattering from the increasingly rough surface. This is ascribed to hydrodynamical processes, such as fluid flow of the surface melt due to surface tension gradients, as well to collapse of cavitation bubbles [30]. The presence of precursor sites significantly alters the energy distribution of subsequent laser pulses [31].

SEM images in Fig. 5(a–i) show the variation in the surface morphology of peripheral ablated regions of Mo targets, exposed to 1000 laser pulses in ethanol, for various local laser fluences of (a) 0.2 m J cm^{-2}, (b) 0.4 m J cm^{-2}, (c) 0.6 m J cm^{-2}, (d) 0.8 m J cm^{-2}, (e) 1.00 m J cm^{-2}, (f) 1.3 m J cm^{-2}, (g) 1.5 m J cm^{-2}, (h) 1.7 m J cm^{-2}and (i) 1.9 m J cm^{-2}. The growth of LPSS is quite evident for all fluences. However, these micrographs are further divided into three parts. Surface modifications in low fluence regime ranging from 0.2 to 0.6 m J cm^{-2} are shown in Fig. 5(a–c). Fig. 5(a) represents broken,

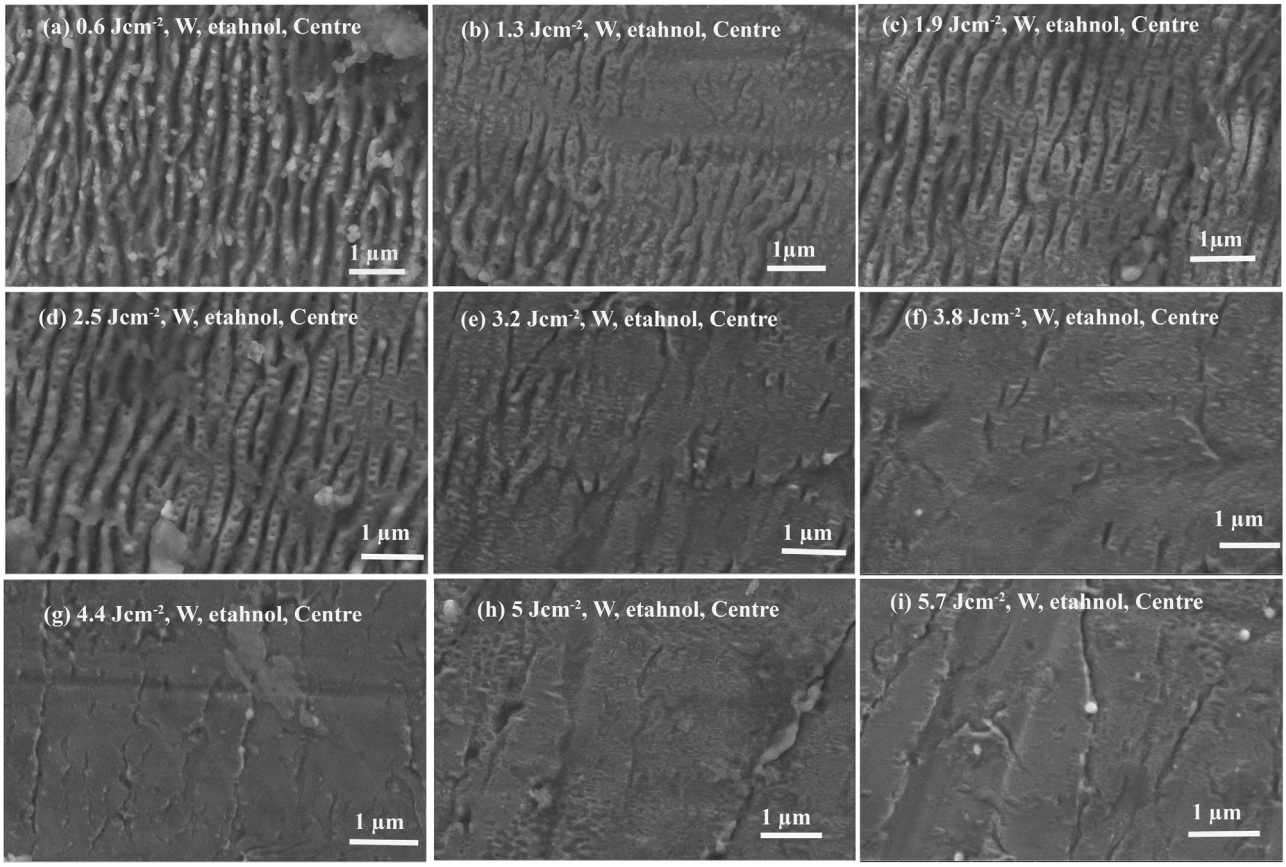

Fig. 2. SEM images revealing the variation in the surface morphology of central ablated regions of W targets, exposed to 1000 laser pulses in ethanol, for various peak laser fluences of (a) 0.6 J cm^{-2}, (b) 1.3 J cm^{-2}, (c) 1.9 J cm^{-2}, (d) 2.5 J cm^{-2}, (e) 3.2 J cm^{-2}, (f) 3.8 J cm^{-2}, (g) 4.4 J cm^{-2}, (h) 5 J $cm^{-2}$and (i) 5.7 J cm^{-2}.

indistinct and substantially unorganized LIPSS. In Fig. 5(b) LIPSS become comparatively distinct and bifurcated. For a fluence of 0.6 m J cm^{-2}, LIPSS become more organized and distinct in Fig. 5(c). The surface modifications at moderate fluence regime ranging from 0.8 to 1.3 m J cm^{-2} are shown in Fig. 5(d–f). At this fluence regime, LIPSS are more distinct and organized as compared to low fluence regime. The periodicity of LIPSS decreases with increasing fluence. The surface modifications at high fluence ranging from 1.5 to 1.9 m J cm^{-2} are shown in Fig. 5(g–i). This fluence is responsible for the growth of highly organized, distinct and well-defined and bifurcated LIPSS.

The formation of holes was found to be highly influenced by the surface inhomogeneities and pre-produced roughness [11]. These holes are the precursors for the chaotic and rugged structures [11].

The LIPSS formation is generally attributed to interaction of the incident laser beam with the excited surface plasmons [14,16,32]. The incoming light can be scattered by microscopic surface roughness, defects, spatial variations in the relative permittivity, etc. Due to the interference pattern, the damage threshold can be periodically exceeded, so that the material melts and resolidifies in the given pattern. The periodic structures on the surface will then act as a grating leading to more light scattering and thereby more energy is coupled to the target. There will be constructive interference in the "valleys" and destructive interference on the "hills", and this positive feedback mechanism causes the growth of ripples [33].

The periodicity of LIPSS is estimated by measuring the distance between two neighboring ripples from SEM micrographs as well as by Fourier Transformation (FT) (Fig. 6b). The dependence of the periodic interspaces on local laser fluence for both W and Mo under fs laser irradiation in ethanol is shown in graph of Fig. 6(c). It is found that the periodicity of LIPSS varies from 310 to 340 nm in case of W and 250–520 nm in case of Mo. These results are compatible with previously reported work by Vorobyev and Guo [25]. According to them [25], LIPSS period for W at a fluence of 0.44 J cm^{-2} vary from 560 to 470 nm, for different numbers of laser pulses ranging from 60 to 800. For W, the periodicity does not change significantly with increasing fluence, but in Mo it increases drastically as the local laser fluence increases, from 0.4 m J cm^{-2} to 0.6 m J cm^{-2}. However, the ripple's period almost remains the same with further increasing laser fluence upto the maximum value of 2.1 m J cm^{-2}. The periodicity of LIPSS is smaller in ethanol as compared to reported values of periodicity in air at similar fluence [16]. This is the clear indication that wet ablation with optimum pulse energy is more suitable for the growth of fine ripples. The rapid adiabatic cooling and fast heat dissipation of ablated region of the W and Mo in the presence of ethanol [30] is a possible reason for the growth of fine ripples in ethanol.

The interspaces of periodic grating structures were in the range from $0.3\lambda_L$ to $0.4\lambda_L$ for W and from $0.3\lambda_L$ to $0.6\lambda_L$ for Mo. Where λ_L is the laser wavelength. This tendency suggests that dependence of variation in interspaces of periodic grating structures on fluence is more pronounced in case of Mo as compared to W. This variation is attributable to strong dependence of surface plasma density on the fluence in Mo than W. This fact leads us to conclude that combination of laser fluence, nature of material and environment play significant role for the growth and periodicity LIPSS [34].

For metals, the surface waves are in the form of Surfce Plasmons (SP,s) that propagate along the metal surface and decay away exponentially from the dielectric/metal interface. The periodicity of LIPSS by surface plasmon's is $\Lambda_{sp}=\lambda_L Re[((\varepsilon_d+\varepsilon_m)/(\varepsilon_d\varepsilon_m))^{1/2}]$, where $\lambda_L$is laser wavelength, ε_d refers to the permittivity of the dielectric medium and $\varepsilon_m= \varepsilon_r+i\varepsilon_i$ is the complex relative permittivity of the metal [25]. The surface plasmons can only exist on a metal/air interface if the metal has a real part of the relative permittivity smaller than −1. Since both W

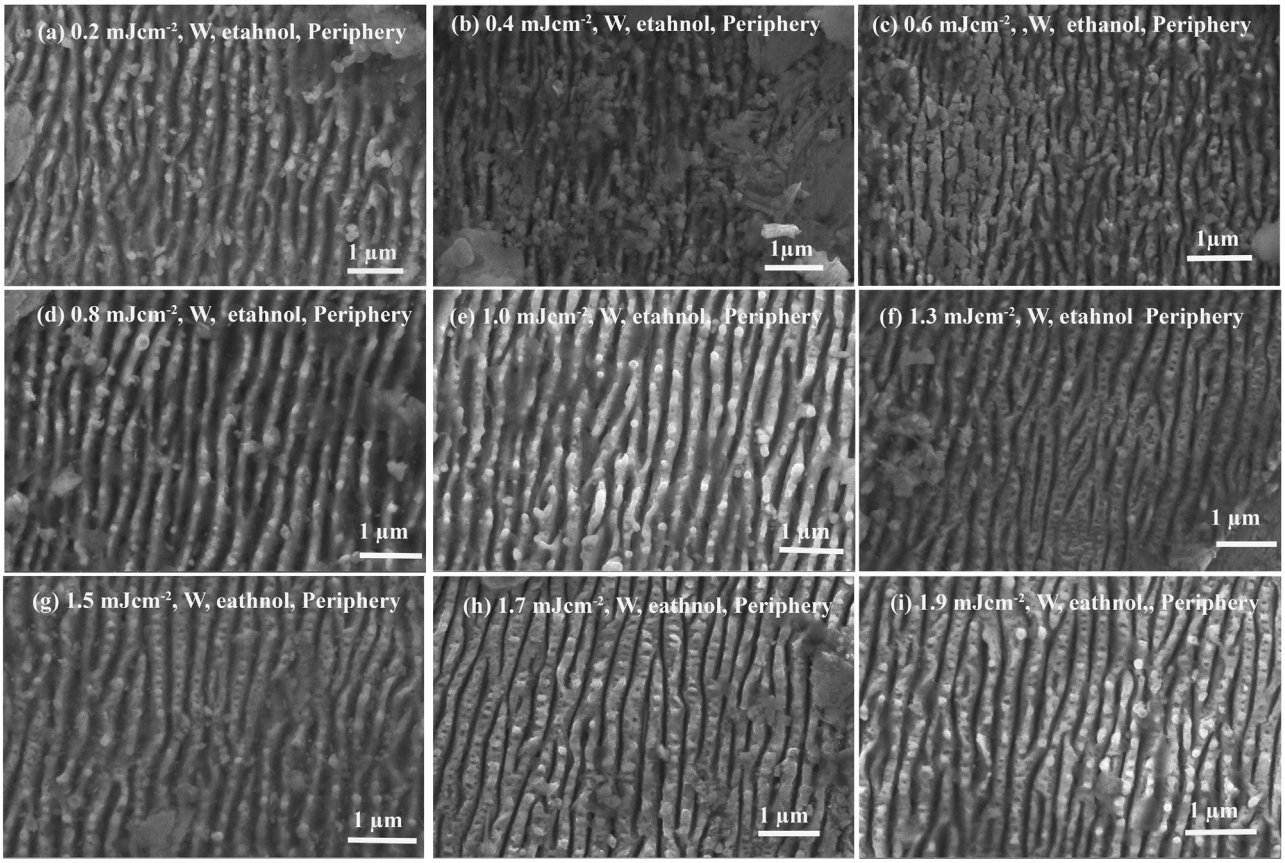

Fig. 3. SEM images revealing the variation in the surface morphology of peripheral ablated regions of W targets, exposed to 1000 laser pulses in ethanol, for various local laser fluences of (a) 0.2 m J cm^{-2}, (b) 0.4 m J cm^{-2}, (c) 0.6 m J cm^{-2}, (d) 0.8 m J cm^{-2}, (e) 1.00 m J cm^{-2}, (f) 1.3 m J cm^{-2}, (g) 1.5 m J cm^{-2}, (h) 1.7 m J cm^{-2} and (i) 1.9 m J cm^{-2}.

and Mo have a positive value at 800 nm ($\varepsilon_r^{W,800nm}$=5, . 22,($\varepsilon_r^{Mo,800nm}$=1.9)and thereby does not support surface plasmons [35]. The surface structures at nanoscale are developed before LIPSS formation can significantly modify the refractive index of W and Mo surface and possibly bring the real part of the relative permittivity below −1. [25].

The non-monotonous behavior of the periodicity of LIPPS with fluence is attributable to different ejecting velocities of the molten material, different angles of the ejection flow and the different rate of evaporation for each fluence. For relatively low fluence, the ejection velocity of the melt is smaller than that caused by higher fluence [36]. But at higher fluences angle of the ejection flow and the rate of evaporation increases nonmonotonically. Similarly the absorption of laser energy by the target surface is also non-monotonous for different fluences. It depends upon the electron number density as well as temperature of ambient plasma, ablation threshold, physical properties and incubation coefficient of target for multi-pulse irradiation.

Characteristics of the laser-produced plasma strongly depend on the laser irradiance levels [37]. As the laser irradiance increases, the number of free electrons increases and consequently there is an increase in the electron density [38]. It is generally believed that the electron density generated at the surface of the bulk material decides the ripple's period, and the electron density is proportional to the laser energy fluence. Both Chakravarty et al. and Xie et al. [39] have confirmed that the ripple's period is relatively larger when the electron density is high. Once a high free electron density is produced by multiphoton ionization, the material has the properties of plasma and will absorb the laser energy via one-photon absorption mechanism of inverse bremsstrahlung (joule) heating. The light absorption in the electron plasma will excite bulk electron plasma density waves.

With increase in laser irradiance, the electron temperature also increases up to a certain irradiance and then saturates [39]. The saturation in electron density and temperature at certain irradiance levels (high fluence in case of Mo and all fluences ranges in case of W) can be explained only on the prominent absorption mechanisms via inverse bremsstrahlung and photoionization. For both fs and ns laser at higher fluences (higher than ablation threshold) and higher pressures (greater than atmospheric) collisional excitation and confinement effects become significantly effective. These effects are responsible for enhancement of laser plasma coupling through inverse bremsstrahlung. At lower pressure levels of environments (less than atmospheric pressures), the trend of excitation temperature of fs-Laser Ablation (LA) is found to be different compared to ns-LA. This difference is due to the fact that for ns-LA, the background pressure affects the laser–target and laser–plasma couplings as well as the plume excitation, confinement mechanisms and shielding effect. However, the ambient environment plays a more significant role in the case of fs-LA, by collisional excitation and confinement. Therefore, the changes in temperature of the fs-LA plume are marginal compared to ns- laser ablation at higher pressures [40]. Along with temperature increase, the ambient environmental confinement will lead to electron density enhancement [41] which in turn enhances the laser–plasma coupling (reheating) through inverse Bremsstrahlung which has a dependence of (electron density) ^{2}.

Such temperature and density behavior can be explained by assuming self-regulating regime. At high irradiance levels, when an appreciable amount of energy is absorbed by the plasma, a self-regulating regime may be formed near the target surface. If the absorption of the laser photons by the plasma becomes higher because of high plasma density, the evaporation of the species from the target becomes less, which in turn decreases the density of the charged species. which in turn increases the temperature of the plasma. On the other hand, when the absorption of the laser energy reduces, the process is reversed, with similar results. The density, temperature, and

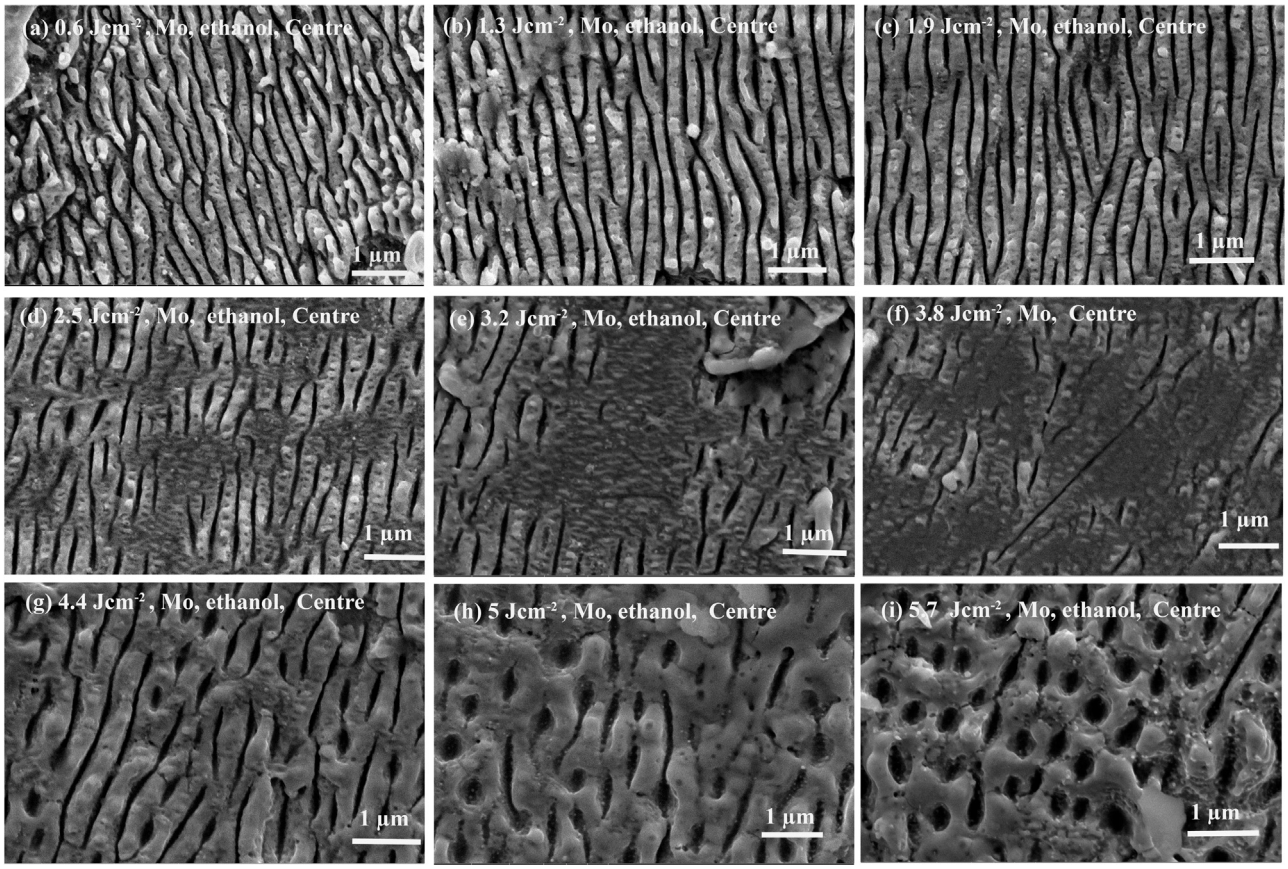

Fig. 4. SEM images revealing the variation in the surface morphology of central ablated regions of Mo targets, exposed to 1000 laser pulses in ethanol, for various peak laser fluences of (a) 0.6 J cm^{-2}, (b) 1.3 J cm^{-2}, (c) 1.9 J cm^{-2}, (d) 2.5 J cm^{-2}, (e) 3.2 J cm^{-2}, (f) 3.8 J cm^{-2}, (g) 4.4 J cm^{-2}, (h) 5 J cm^{-2}and (i) 5.7 J cm^{-2}.

dimensions of the plume adjust in such a manner that the plasma absorbs the same amount of laser radiation to maintain a self-regulating regime [42].

For W by increasing fluence no significant change in periodicity is observed. This can be attributed to high melting point, thermal conductivity, thermal diffusivity and enthalpy of evaporation for W than Mo. The generation of free-carriers, leads to an interplay between diffusive transport and impact ionization. When self-regulating regime is reached then with further increase in fluence no more enhancement of periodicity of ripples occurs [15].

The laser beam was focused onto the target through a liquid layer of about 5 mm millimeters in thickness through the ill-defined air-liquid interface without the use of a window or a clear side of the cuvette. When the beam focus passes through ethanol, various nonlinear effects [1] as well as filamentation and self-phase modulation occur. Of course all these phenomenon are responsible for broadening of spectrum inside the liquid. The pulse stretching inside the liquids can be considered additional effects induced by liquid during ablation of W and Mo. Nonlinear optical effects occurring in the surrounding environment induced by fs laser pulses influence the refractive index. Surface nano-texturing is accompanied by changes in the absorption spectrum of the target material, in the surface wettability, and surface enhanced Raman scattering (SERS) properties [43,44].

The interaction of the laser beam with target surface at the fluence greater than the ablation threshold of the material, results in the ablation (removal) of the material in the form of a plasma plume. The high temperature of the plume results in the ionization and vaporization of the liquid at the plume–liquid interface and its conversion into ethanol vapor, atomic and molecular carbon, hydrogen or oxygen (ethanol plasma). This liquid plasma fuses with the plume plasma and causes chemical reactions to take place between the ethanol plasma and the ablated species plasma. In case of liquid assisted ablation as compared to ablation in vacuum or a controlled gas atmosphere, plasma expands adiabatically with super-sonic velocity within the liquid in which the target is immersed, and experiences an additional confinement effect from the liquid. Also a shock wave is generated at the plume–liquid interface which travels back and forth within the plume. These effects are responsible to increase the temperature, pressure and density of the plume.

The ablation threshold is a key parameter for discussing the mechanism of self-organized grating structure formations. A simple theoretical value for the single-shot threshold fluence is found by assuming that the light is absorbed according to Beer's law (exponentially with a characteristic absorption length $1/\alpha$). The ablation occurs when the energy per unit volume exceeds the energy necessary for the material to undergo heating, melting and evaporation. This energy can often be well approximated by its dominating term, the enthalpy of evaporation per unit volume $\rho\Omega_{\mathrm{vap}}$. By taking this into consideration only a fraction A of the light is actually absorbed, the threshold fluence can be expressed [35].

$$F_{th} = \frac{\rho\Omega_{vap}}{\alpha A} \quad (2)$$

The theoretical values of threshold fluences from relation (2) and tabulated values of Table 1 come out to be 0.44 J cm^{-2} and 0.32 J cm^{-2} for W and Mo, respectively which are also listed in Table 1.

The two regimes in laser ablation are the multi-photon (skin depth) and the electron diffusion (thermal). The optical penetration depth (l_{opt}) $1/\alpha$(nm) is 23.6 [35] and 18.9 [45] for W and Mo respectively for 800 nm wavelength. The thermal diffusion depth is $l_{th}\sim\sqrt{\chi\tau}$, where $\chi = \frac{K}{\rho C}$, is thermal diffusivity, K is thermal conductivity, ρ is density and C is specific heat capacity of the material. The thermal diffusion

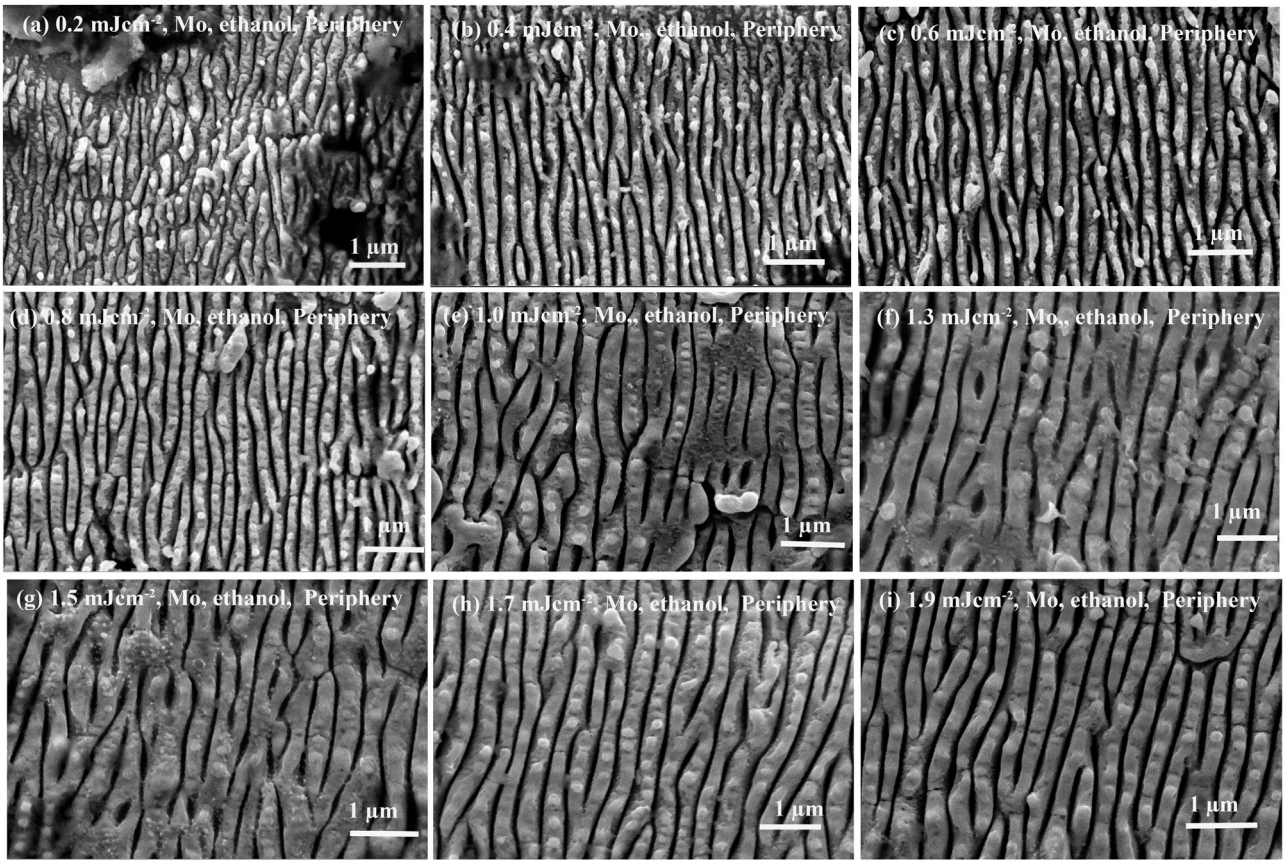

Fig. 5. SEM images revealing the variation in the surface morphology of peripheral ablated regions of Mo targets, exposed to 1000 laser pulses in ethanol, for various local laser fluences of (a) 0.2 m J cm^{-2}, (b) 0.4 m J cm^{-2}, (c) 0.6 m J cm^{-2}, (d) 0.8 m J cm^{-2}, (e) 1.0 m J cm^{-2}, (f) 1.3 m J cm^{-2}, (g) 1.5 m J cm^{-2}, (h) 1.7 m J cm^{-2} and (i) 1.9 m J cm^{-2}.

depth $l_{th}(\mu m)$ is 1.4 µm [46] and 11.27 µm [46] for W and Mo respectively.

The experimental values of ablation depth for both W and Mo at various fluences are measured by using confocal microscope. The confocal microscopy images for (a) 2D profile (b) 3D profile and corresponding (c) section profile are shown in Fig. 7. It corresponds to Mo surface exposed to 1000 laser shots in ethanol at a fluence of 3.2 J cm^{-2}.

The plot of ablation depth Vs fluence is shown in Fig. 8(a) for both W and Mo. It clearly indicates that ablation depth increases lineally with increasing fluence. The values of ablation depth varies from 1 to 9 µm for W and from 3 to 22 µm for Mo with the fluence variation from 0.6 to 5.7 J cm^{-2}. The effective ablation depth (for 1000 pulses in ethanol environment) is significantly higher than both optical penetration and thermal penetration depth. It is attributable to multiple laser irradiation as well as confinement effects of ethanol.

When the target is ablated with signal shot, its fundamental and unaltered physical and thermal properties are responsible for its ablation. However, with multiple shots, accumulation behavior plays a significant role. The accumulated deposited energy per unit volume significantly increases by increasing number of pulses [47]. Therefore the incubation effect increases with increasing laser pulses and correspondingly laser threshold fluence decreases. Another important factor is the enhancement of energy coupling efficiency, which may be related to the decrease in the reflectivity of the incident laser pulse [48] Initial pulses are also responsible for the generation of defects in the target material. The intensity of the electric field of incoming laser light and its absorption is also enhanced due to this defect generated

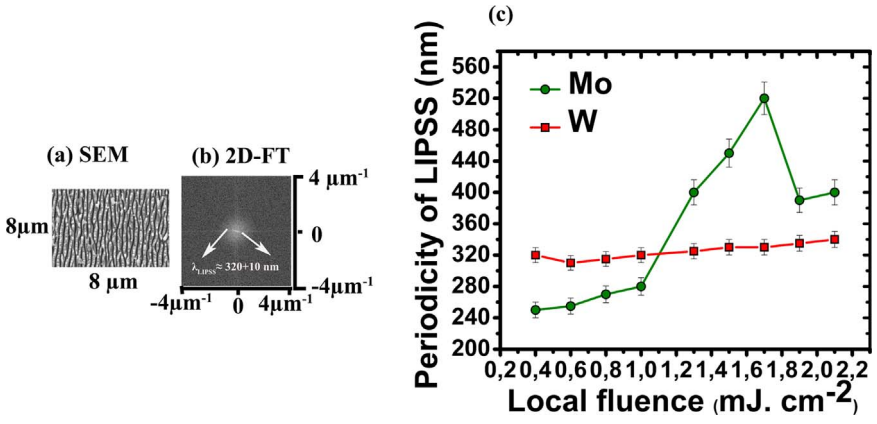

Fig. 6. The periodicity of the ripples measured by Fourier Transformation (FT) (a) SEM micrograph (b) Corresponding 2D-FT of Mo surface after irradiation with 1000 fs-laser pulses in ethanol. (c) The dependence of the periodic structure interspaces on local laser fluence for both W and Mo under fs laser irradiation in ethanol.

Table 1
Some Important thermal, physical and optical properties of W and Mo.

Some important thermal, physical and optical properties	W	Mo
Enthalpy of evaporation $(\Delta H_v)GJ/m^3$	86.5 [35]	78 [55]
Work function (eV)	4.55 [56]	4.66 [56]
$\alpha(10^5 cm^{-1})$	4.2373 [35]	5.2856 [45]
Optical penetration depth (l_{opt}) $1/\alpha$(nm)	23.6 [35]	18.9 [45]
Absorption (A)	0.5 [35]	0.45 [45]
Refractive index (n)	3.65 [45]	3.63 [45]
Extinction coefficient (k)	2.69 [45]	3.36 [45]
Relative permittivity ϵ_1	5.22 [35]	1.9059 [45]
Relative permittivity ϵ_2	19.905 [45]	24.477 [45]
Thermal diffusion depth $l_{th(\mu m)}$	1.4 [46]	1.27 [46]
Melting point °C	3422 [46]	2623 [46]
Boiling Temperature °C	5700 [46]	4639 [46]
Density ρ(g/cm^3)	19.25 [46]	10.22 [46]
Thermal Conductivity (W m^{-1} K^{-1})	170 [46]	139 [46]
Specific Heat capacity (J Kg^{-1} K^{-1})	135 [46]	251 [46]
Thermal diffusivity χ(mm^2/sec)	65 [46]	54 [46]
$\frac{\Delta H_v}{\alpha A}(J/cm^2)$Threshold Fluence Theoretical [35]	0.44 ± 0.2	0.32 ± 0.2
Threshold Fluence Experimental for 1000 laser pulses in ethanol	$F_{th,\ Ethanol}$=88 m J cm^{-2}	$F_{th\ Ethanol}$ = 35 mJ cm^{-2}

enhanced surface roughness and exhibits an accumulation behavior. The excitations of the surface plasmons also play a significant role as they may provide extra energy in coupling mechanism [48]. As the laser radiation absorption of the sample increases significantly during multi-pulse ablation [49,50], therefore accumulation and incubation effects by multipulse irradiation cause significant reduction in observed F_{th} [51].

The fluence dependent crater diameter was determined by SEM analysis. With Gaussian distribution of laser beam the crater diameter is expressed as follows [52].

$$F_{th} = Fexp\left\{-\left(\frac{\Gamma}{a}\right)^2\right\} \quad (3)$$

where Γ is the crater diameter, a is the laser beam diameter. The plot of the squared cavity diameter in dependence of applied fluence for both W and Mo is shown in Fig. 8(b).

The ablation threshold was roughly estimated by the laser fluence resulting in minimal crater diameter. The experimental values of threshold for 1000 multiple pulses come out to be $F_{th,\ W,\ Ethanol}$ =88 m J cm^{-2} and $F_{th,\ Mo,\ Ethanol}$=35 m J cm^{-2}. It is observed that threshold fluence for W is higher than Mo. It is attributable to high value of enthalpy of evaporation, melting point, boiling point of W than Mo (see Table 1).

In the presence of liquids the chemical reactivity of the target with liquid is significantly enhanced which is responsible for the growth of new phases and modification in the chemical composition of the irradiated target. The extremely high pressure in front of the laser-induced plasma will impinge the ablation species from the solid target at the plasma–liquid interface into the liquid, and then, the chemical reactions between the ablation species and the liquid molecules will occur inside the liquid [53]. Our values are also significantly smaller than reported values by Gemini et al. [54] according to which the ablation threshold fluence for 100 pulses for Mo and W is 0.29 and 0.13 Jcm^{-2} respectively. The lower limit fluences at which classical ripples begin to form are 0.46 and 0.18 J cm^{-2}and upper limit fluence above which they are no longer generated is 1.1 J cm^{-2} for both metals. Again the reason behind this reduced ablation threshold is 10 times higher number of pulses (1000 as compared to 100).

4. Conclusions

The effect of increasing laser fluences of fs laser on formation of nano structures on W and Mo surfaces after irradiation in ambient environment of ethanol has been investigated. It is concluded that laser fluence, irradiation environment and nature of material play important role for the growth of nanoscale surface structures. In case of central areas, for W, nonuniform and unorganized LIPSS are formed for low fluences ranging from 0.6 to 2.5 J cm^{-2}, whereas, nonuniform melting and cracking has occurred for higher fluences ranging from 3.2 to 5.7 J cm^{-2}. For the peripheral ablated areas, LIPSS for all fluences are produced. However, the dependence of periodicity on fluence is more pronounced for Mo than W. The ablation depth and crater diameter for

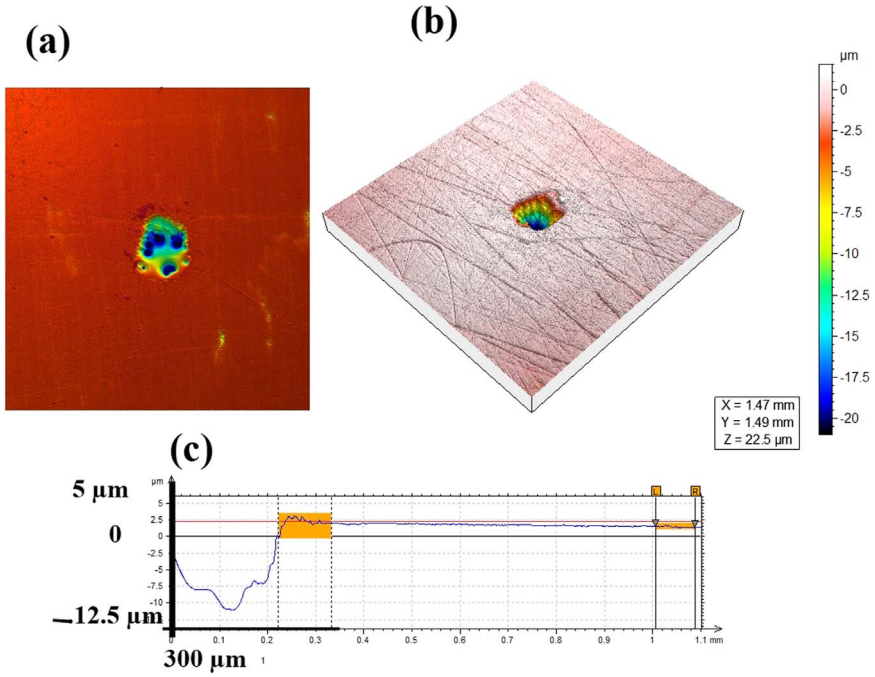

Fig. 7. The confocal microscopy images for (a) 2D profile (b) 3D profile and corresponding (c) section profile of Mo exposed to 1000 laser shots in ethanol at a fluence of 3.2 J cm^{-2}.

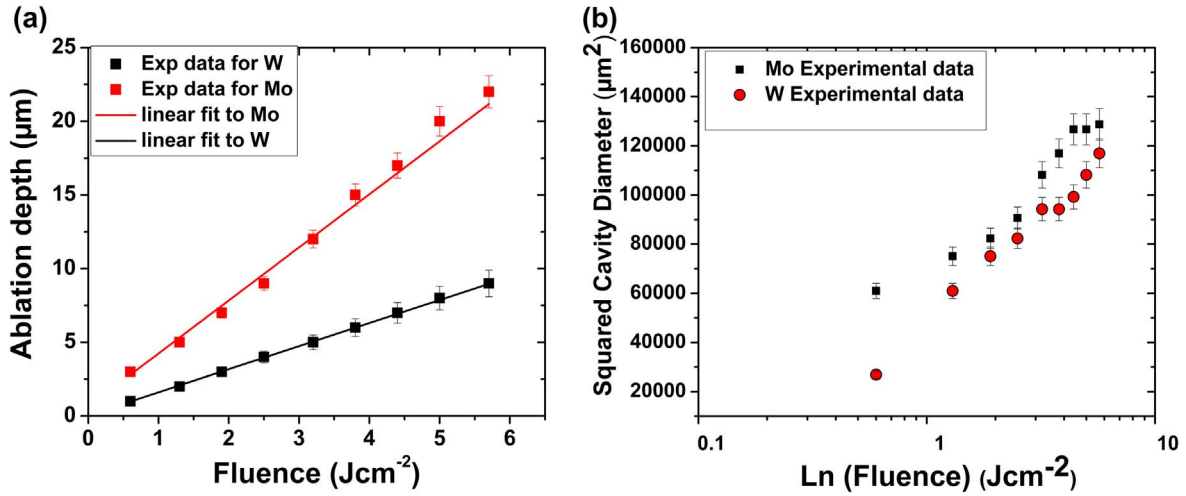

Fig. 8. (a) The plot of ablation depth Vs fluence for both W and Mo, (b) The plot of the squared cavity diameter in dependence of applied fluence for both W and Mo.

both the metals show increasing trend with increase in the laser fluence due to more energy deposition at the surface. However, the threshold fluence for W is higher than Mo.

References

[1] Y. Yang, J. Yang, C. Liang, H. Wang, Ultra-broadband enhanced absorption of metal surfaces structured by femtosecond laser pulses, Opt. Exp. 16 (2008) 11259–11265.

[2] E.V. Barmina, A.A. Serkov, E. Stratakis, C. Fotakis, V.N. Stolyarov, I.N. Stolyarov, G.A. Shafeev, Nano-Textured W shows improvement of thermionic emission properties, Appl. Phys. A 106 (2012) 1.

[3] A.Y. Vorobyev, V.S. Makin, C. Guo, Brighter light sources from black metal: significant increase in emission efficiency of incandescent light sources, Phys. Rev. Lett. 102 (2009) 234301.

[4] J. Bekesi, J. Kaakkunen, W. Michaeli, F. Klaiber, M. Schoengart, J. Ihlemann, P. Simon, Fast fabrication of super-hydrophobic surfaces on polypropylene by replication of short-pulse laser structured molds, Appl. Phys. A 99 (2010) 691.

[5] Y. Yang, J. Yang, C. Liang, H. Wang, X. Zhu, N. Zhang, Surface microstructuring of Ti plates by femtosecond lasers in liquid ambiences: a new approach to improving biocompatibility, Opt. Exp. 17 (2009) 21124.

[6] J. Bonse, R. Koter, M. Hartelt, D. Spaltmann, S. Pentziea, S. Höhm, A. Rosenfeld, J. Krüger, Appl. Surf. Sci. 336 (2015) 21.

[7] S. Bashir, M.S. Rafique, C.S.R. Nathala, A. Ajami, W. Husinsky, SEM and Raman spectroscopy analyses of laser induced periodic surface structures grown by ethanol assisted femtosecond laser ablation of chromium, Radiat. Eff. Defects Solids 170 (5) (2015) 414.

[8] S. Moradi, S. Kamal, P. Englezos, S.G. Hatzikiriakos, Femtosecond laser irradiation of metallic surfaces: effects of laser parameters on superhydrophobicity, Nanotechnology 24 (2013) 415302.

[9] M. Shimizu, M. Hashida, Y. Miyasaka, S. Tokita, S. Sakabe, Unidirectionally oriented nanocracks on metal surfaces irradiated by low-fluence femtosecond laser pulses, Appl. Phys. Lett. 103 (2013) 174106.

[10] M.J. Abere, C. Chen, D.R. Rittman, M. Kang, R.S. Goldman, J.D. Phillips, B. Torralva, S.M. Yalisove, Nanodot formation induced by femtosecond laser irradiation, Appl. Phys. Lett. 105 (2014) 163103.

[11] K. Kurselis, R. Kiyan, B.N. Chichkov, Formation of corrugated and porous steel surfaces by femtosecond laser irradiation, Appl. Surf. Sci. 258 (2012) 8845.

[12] H. Zhang, G. Duan, Y. Li, X. Xu, Z. Dai, W. Cai, Leaf-like tungsten oxide nanoplatelets induced by laser ablation in liquid and subsequent aging, Cryst. Growth Des. 12 (2012) 2646.

[13] M. Birnbaum, Semiconductor surface damage produced by Ruby lasers, J. Appl. Phys. 36 (1965) 3688.

[14] J.F. Young, J.S. Preston, H.M. Van Driel, J.E. Sipe, Laser-induced periodic surface structure. II. Experiments on Ge, Si, Al, and brass, Phys. Rev. B 27 (1983) 1155.

[15] S. Sakabe, M. Hashida, S. Tokita, S. Namba, K. Okamuro, Mechanism for self-formation of periodic grating structures on a metal surface by a femtosecond laser pulse, Phys. Rev. B - Condens. Matter Mater. Phys. 79 (3) (2009) 033409.

[16] T.J.-Y. Derrien, R. Koter, J. Krüger, S. Höhm, A. Rosenfeld, J. Bonse, Plasmonic formation mechanism of periodic 100-nm-structures upon femtosecond laser irradiation of silicon in water, J. Appl. Phys. 116 (2014) 074902.

[17] G.H. Welsh, N.T. Hunt, K. Wynne, Terahertz-pulse emission through laser excitation of surface plasmons in a metal grating, Phys. Rev. Lett. 98 (2007) 026803.

[18] A.Y. Vorobyev, C. Guo, Nanochemical effects in femtosecond laser ablation of metals, Appl. Phys. Lett. 102 (2013) 074107.

[19] S. Bashir, M.S. Rafique, W. Husinsky, Liquid assisted ablation of zirconium for the growth of LIPSS at varying pulse durations and pulse energies by femtosecond laser irradiation, Nucl. Instrum. Method B 349 (2015) 230.

[20] E.V. Barmina, A.A. Serkov, E. Stratakis, C. Fotakis, V.N. Stolyarov, I.N. Stolyarov, G.A. Shafeev, Laser-assisted nano-texturing of W substrates cathodes via ablation in liquid environment, Appl. Phys. A 106 (2012) 1.

[21] S. Bashir, M.S. Rafique, C.S. Nathala, W. Husinsky, Surface and structural modifications of titanium induced by various pulse energies of a femtosecond laser in liquid and dry environment, Appl. Phys. A 114 (2014) 243.

[22] H. Zhang, S.B. Lu, J. Zheng, J. Du, S.C. Wen, D.Y. Tang, K.P. Loh, Molybdenum disulfide (MoS_2) as a broadbandsaturable absorber for ultra-fast photonics, Opt. Exp. 22 (2014) 7251.

[23] J.G. Fujimoto, J.M. Liu, E.P. Ippen, N. Bloembergen, Phys. Rev. Lett. 53 (1984) 1837.

[24] H. Zhang, M. Tang, J. McCoy, T.H. Her, Deposition of tungsten nanogratings induced by a single femtosecond laser beam, Opt. Exp. 15 (2007) 5937.

[25] A.Y. Vorobyev, C. Guo, Femtosecond laser-induced periodic surface structure formation on tungsten, J. Appl. Phys. 104 (2008) 063523.

[26] M. Tang, H. Zhang, T.H. Her, Nanotechnology 18 (2007) 485304.

[27] J. Cong, J. Yang, B. Zhao, X. Xu, Fabricating subwavelength dot-matrix surface structures of Molybdenum by transient correlated actions of two-color femtosecond laser beams, Opt. Exp. 23 (2015) 5358.

[28] J. Bonse, J. Krüger, Pulse number dependence of laser-induced periodic surface structures for femtosecond laser irradiation of silicon, J. Appl. Phys. 108 (2010) 034903.

[29] M. Shimizu, M. Hashida, Y. Miyasaka, S. Tokita, S. Sakabe, Unidirectionally oriented nanocracks on metal surfaces irradiated by low-fluence femtosecond laser pulses, Appl. Phys. Lett. 103 (2013) 174106.

[30] L.M.J. Santillán, F.A. Videla, M.B. Fernández van Raap, D.C. Schinca, L.B. Scaffardi, Analysis of the structure, configuration, and sizing of Cu and Cu oxide nanoparticles generated by fs laser ablation of solid target in liquids, J. Appl. Phys. 113 (2013) 134305.

[31] A.Y. Vorobyev, C. Guo, Enhanced absorptance of gold following multipulse femtosecond laser ablation, Phys. Rev. B 72 (2005) 1.

[32] S. Höhm, M. Herzlieb, A. Rosenfeld, J. Krüger, J. Bonse, Laser-induced periodic surface structures on fused silica upon cross-polarized two-color double-fs-pulse irradiation, Appl. Surf. Sci. 336 (2015) 39.

[33] J. Reif, O. Varlamova, F. Costache, Femtosecond laser induced nanostructure formation: self-organization control parameters, Appl. Phys. A 92 (2008) 1019.

[34] K. Okamuro, M. Hashida, Y. Miyasaka, Y. Ikuta, S. Tokita, S. Sakabe, Laser fluence dependence of periodic grating structures formed on metal surfaces under femtosecond laser pulse irradiation, Phys. Rev. B 82 (2010) 165417.

[35] J. Byskov-Nielsen, J.M. Savolainen, M.S. Christensen, P. Balling, Ultra-short pulse laser ablation of metals: threshold fluence, incubation coefficient and ablation rates, Appl. Phys. A 101 (2010) 97.

[36] K.C. Yung, S.M. Mei, T.M. Yue, Pulsed UV laser ablation of a liquid crystal polymer, Int. J. Adv. Manuf. Technol. 26 (2005) 1231.

[37] S.S. Harilal, C.V. Bindhu, V.P.N. Nampoori, C.P.G. Vallabhan, Temporal and spatial behavior of electron density and temperature in a laser -produced plasma from $YBa_2Cu_3O_7$, Appl. Spect. 52 (1998) 449.

[38] S.S. Harilal, C.V. Bindhu, Riju C. Issac, V.P.N. Nampoori, C.P.G. Vallabhan, Electron density and temperature measurements in a laser produced carbon plasma, J. Appl. Phys. 82 (1997) 2140.

[39] U. Chakravarty, P.A. Naik, J.A. Chakera, A. Upadhyay, P.D. Gupta, Estimation of electron density and temperature of semiconductor surfaces excited by ultra-short laser pulses, Appl. Phys. A 115 (2014) 1457.

[40] S.S. Harilal, N. Farid, J.R. Freeman, P.K. Diwakar, N.L. LaHaye, A. Hassanein, Background gas collisional effects on expanding fs and ns laser ablation plumes, Appl. Phys. A 117 (2014) 319.

[41] J.R. Freeman, S.S. Harilal, P.M. Diwakar, B. Verhoff, A. Hassanein, Comparison of optical emission from nanosecond and femtosecond laser produced plasma in atmosphere and vacuum conditions, Spectrochim. Acta B 87 (2013) 43.

[42] A. Caruso, R. Gratton, Interaction of short laser pulses with solid material, Plasma Phys. 10 (1968) 867.
[43] E.V. Barmina, E. Stratakis, M. Barberoglou, V.N. Stolyarov, I.N. Stolyarov, C. Fotakis, G.A. Shafeev, Laser-assisted nanostructuring of Tungsten in liquid environment, Appl. Surf. Sci. 258 (2012) 5898.
[44] B.N. Chichkov, C. Momma, S. Nolte, F. Von Alvensleben, A. TuÌnnermann, Femtosecond, picosecond and nanosecond laser ablation of solids, Appl. Phys. A 63 (1997) 109.
[45] M.A. Ordal, R.J. Bell, R.W. Alexander Jr., L.A. Newquist, M.R. Querry O, Optical properties of Al, Fe, Ti, Ta, W, and Mo at submillimeter wavelengths, Appl. Opt. 27 (1988) 1203.
[46] ⟨http://periodictable.com/Properties/A/BoilingPoint.al.html⟩.
[47] P.T. Mannion, J. Magee, E. Coyne, G.M. O'Connor, T.J. Glynn, The effect of damage accumulation behaviour on ablation thresholds and damage morphology in ultrafast laser micro-machining of common metals in air, Appl. Surf. Sci. 233 (2004) 275.
[48] J. Byskov-Nielsen, J.M. Savolainen, M.S. Christensen, P. Balling, Ultra-short pulse laser ablation of metals: threshold fluence, incubation coefficient and ablation rates, Appl. Phys. A 97 (2010) 97.
[49] A. Rosenfeld, M. Lorenz, R. Stoian, D. Ashkenasi, Ultrashort-laser-pulse damage threshold of transparent materials and the role of incubation, Appl. Phys. A 69 (1999) S373.
[50] N. Yaseen, S. Bashir, M. Akram, A. Hayat, M.K. Shabbir, S.A. Jalil, F.U. Haq, R. Ahmad, T. Hussian, Nanosecond pulsed laser ablation of Ge investigated by employing photoacoustic deflection technique and SEM analysis, Phys. B 490 (2016) 31.
[51] U. Kalsoom, S. Bashir, N. Ali, M.S. Rafique, W. Husinsky, C.S.R. Nathala, S.V. Makarov, N. Begum, The effect of fluence and ambient environment on the surface and structural modification of femtosecond laser irradiated Ti, Chin. Phys. B 25 (2016) 018101.
[52] J. Jandeleit, G. Urbasch, H.D. Hoffmann, H.G. Treusch, E.W. Kreutz, Picosecond laser ablation of thin copper films, Appl. Phys. A 63 (1996) 117–121.
[53] G.W. Yang, Laser ablation in liquids: applications in the synthesis of nanocrystals, Prog. Mat. Sci. 52 (2007) 648.
[54] L. Gemini, M. Hashida, M. Shimizu, Y. Miyasaka, S. Inoue, S. Tokita, J. Limpouch, T. Mocek, S. Sakabe, Metal-like self-organization of periodic nanostructures on silicon and silicon carbide under femtosecond laser pulses, J. Appl. Phys. 114 (2013).
[55] G. Heise, M. Englmaier, C. Hellwig, T. Kuznicki, S. Sarrach, H.P. Huber, Laser ablation of thin molybdenum films on transparent substrates at low fluences, Appl. Phys. A 102 (2011) 173.
[56] T. Li, B.L. Rickman, W.A. Schroeder, Emission properties of body-centered cubic elemental metal photocathodes, J. Appl. Phys. 117 (2015) 134901.